

# Dynamical bar-mode instability of differentially rotating stars: Effects of equations of state and velocity profiles

Masaru Shibata, Shigeyuki Karino, and Yoshiharu Eriguchi

*Department of Earth Science and Astronomy, Graduate School of Arts and Sciences, University of Tokyo, Komaba, Meguro, Tokyo 153-8902, Japan*

Accepted ???? Month ??, Received ???? Month ??; in original form 2002 April 1

## ABSTRACT

As an extension of our previous work, we investigate the dynamical instability against nonaxisymmetric bar-mode deformations of differentially rotating stars in Newtonian gravity varying the equations of state and velocity profiles. We performed the numerical simulation and the followup linear stability analysis adopting polytropic equations of state with the polytropic indices  $n = 1, 3/2$ , and  $5/2$  and with two types of angular velocity profiles (the so-called  $j$ -constant-like and Kepler-like laws). It is confirmed that rotating stars of a high degree of differential rotation are dynamically unstable against the bar-mode deformation, even for the ratio of the kinetic energy to the gravitational potential energy  $\beta$  of order 0.01. The criterion for onset of the bar-mode dynamical instability depends weakly on the polytropic index  $n$  and the angular velocity profile as long as the degree of differential rotation is high. Gravitational waves from the final nonaxisymmetric quasi-stationary states are calculated in the quadrupole formula. For proto-neutron stars of mass  $1.4M_{\odot}$ , radius  $\sim 30$  km and  $\beta \lesssim 0.1$ , such gravitational waves have the frequency of  $\sim 600$ – $1,400$  Hz, and the effective amplitude is larger than  $10^{-22}$  at a distance of about 100 Mpc irrespective of  $n$  and the angular velocity profile.

**Key words:** gravitational waves – stars: neutron – stars: rotation – stars: oscillation.

## 1 INTRODUCTION

In our previous paper, we studied dynamical bar-mode stabilities of differentially rotating stars in Newtonian gravity (Shibata et al. 2002). In that study, we adopted a polytropic equation of state with the polytropic index  $n = 1$  and the so-called “ $j$ -constant-like” angular velocity profile in which the magnitude of the angular velocity decreases as  $\varpi^{-2}$  at large values of  $\varpi$ , where  $\varpi$  denotes the cylindrical radius. We found that rotating stars of a high degree of differential rotation are dynamically unstable even for  $\beta \equiv |T/W| \sim 0.03$ , where  $T$  and  $W$  are rotational and gravitational potential energies. This value is much smaller than the long-believed criterion of  $\beta \approx 0.27$  for onset of the bar-mode dynamical instability of rotating stars (see Shibata et al. 2002 for a review). We also found that after the instability sets in, such unstable rotating stars with  $0.03 \lesssim \beta \lesssim 0.15$  eventually settle down to nonaxisymmetric ellipsoidal quasi-stationary states.

However, there are two questions which have not been answered in the previous work (Shibata et al. 2002). One is associated with our choice of the  $j$ -constant-like angular velocity profile. It is well known that accretion disks around

a central body with constant specific angular momentum are unstable against the Papaloizou-Pringle instability (Papaloizou & Pringle 1984). On the other hand, the accretion disks are stable if the velocity profile is Kepler-like. One could claim that the bar-mode instability which we found would not be universal and might set in only for the very special rotational profile such as the  $j$ -constant-like law as in the Papaloizou-Pringle instability. In addition, we focused only on a stiff equation of state with  $n = 1$  in the previous paper, so that one could also ask if the instability sets in for softer equations of state.

To answer these questions, we have performed numerical simulations of differentially rotating stars varying the polytropic index and the angular velocity profile. In this paper, we report the numerical results. We will show that irrespective of the polytropic index  $n$  and the angular velocity profile, a rotating star of a high degree of differential rotation is dynamically unstable against the bar-mode deformation even for the case that  $\beta$  is of order 0.01. We will also show that an unstable star of a small value of  $\beta$  eventually settles down to a nonaxisymmetric quasi-stationary state, which is a strong emitter of quasi-periodic gravitational waves.

The paper is organized as follows. In Section 2, we de-

scribe our methods in numerical analysis. In Section 3, the numerical results are presented. Section 4 is devoted to a summary and discussion. Throughout this paper, we use the geometrical units of  $G = c = 1$  where  $G$  and  $c$  denote the gravitational constant and the light velocity.

## 2 METHOD

### 2.1 Differentially rotating axisymmetric stars

We set a differentially rotating star in equilibrium, and investigate the dynamical stability. Rotating stars in equilibrium are modeled using the polytropic equations of state as  $P = K\rho^\Gamma$  where  $P$ ,  $\rho$ ,  $K$  and  $\Gamma = 1 + 1/n$  denote the pressure, density, polytropic constant and adiabatic index. In this paper, we choose  $n = 1, 3/2$ , and  $5/2$  ( $\Gamma = 2, 5/3$ , and  $7/5$ ).

As the angular velocity profile  $\Omega(\varpi)$ , we choose the so-called  $j$ -constant-like law as

$$\Omega = \frac{\Omega_0 A^2}{\varpi^2 + A^2}, \quad (1)$$

and the so-called Kepler-like law as

$$\Omega = \Omega_0 \left[ \frac{A^2}{\varpi^2 + A^2} \right]^{3/4}, \quad (2)$$

where  $A$  is a constant, and  $\Omega_0$  the angular velocity at the symmetric axis. The parameter  $A$  controls the steepness of the angular velocity profile: For smaller values of  $A$ , the profile is steeper and for  $A \rightarrow \infty$ , the rigid rotation is recovered. In the present work, the values of  $A$  are chosen among the range  $0.1 \leq \hat{A} \equiv A/R_{\text{eq}} \leq 1$  where  $R_{\text{eq}}$  is the equatorial radius of rotating stars. For the rotation laws (1) and (2),  $\Omega$  at large cylindrical radius asymptotically behaves as  $\varpi^{-2}$  and  $\varpi^{-3/2}$ . This is the reason why we refer to the profiles (1) and (2) as the  $j$ -constant-like and Kepler-like laws.

In the limit of  $A \rightarrow 0$  with the profile (1), the specific angular momentum becomes constant everywhere and  $\Omega$  diverges at  $\varpi = 0$ . We note that this profile has been often used in studies of nonaxisymmetric instabilities in tori and annuli (Papaloizou & Pringle 1984; Goodman & Narayan 1988; Tohline & Hachisu 1990; Andalib & Tohline 1997). In this paper, however, we do not consider tori and annuli and focus only on spheroidal stars for which the density is not zero at  $\varpi = 0$ . Thus, we cannot adopt this limiting profile.

In terms of  $\beta = T/|W|$  and  $\hat{A}$ , one rotating star is determined for a given rotational profile and polytropic index. Thus, in the following, we often refer to these two parameters to specify a rotating star. Here,  $T$  and  $W$  are defined as

$$T = \frac{1}{2} \int d^3x \rho \varpi^2 \Omega^2, \quad (3)$$

$$W = \frac{1}{2} \int d^3x \rho \phi, \quad (4)$$

where  $\rho$  and  $\phi$  are the mass density and the Newtonian gravitational potential. To specify a particular model, we may choose the axis ratio of the rotating stars  $C_a$  instead of  $\beta$ . Here  $C_a$  is defined as the ratio of the polar radius  $R_p$  to the equatorial radius  $R_{\text{eq}}$ , i.e.,  $C_a = R_p/R_{\text{eq}}$ . For the equations of state and the angular velocity profiles that we study in

this paper, the value of  $C_a$  monotonically decreases with increase of  $\beta$  for a given set of  $\hat{A}$  and  $n$ . This is the reason that  $C_a$  can be a substitute for  $\beta$ .

### 2.2 Dynamical stability investigation

To investigate the dynamical stability against nonaxisymmetric bar-mode deformations, we have performed the numerical simulation as well as the linear stability analysis. Below we explain the methods for our numerical computation separately.

#### 2.2.1 Numerical simulation

In the hydrodynamic simulation, we initially superimpose a nonaxisymmetric density perturbation to an axisymmetric equilibrium star. We focus mainly on a fundamental bar-mode, and simply add the mode-less density perturbation of the form

$$\delta\rho = \delta \cdot \rho_0(\varpi, z) \frac{x^2 - y^2}{R_{\text{eq}}^2}, \quad (5)$$

where  $\rho_0(\varpi, z)$  denotes the density of the axisymmetric configuration and  $\delta$  constant. Throughout this paper, we choose  $\delta = 0.1$ . For simplicity, the velocity is left to be unperturbed at  $t = 0$ . The growth of the bar-mode can be followed by monitoring the distortion parameter as

$$\eta \equiv (\eta_+^2 + \eta_-^2)^{1/2}, \quad (6)$$

where

$$\eta_+ \equiv \frac{I_{xx} - I_{yy}}{I_{xx} + I_{yy}}, \quad (7)$$

$$\eta_- \equiv \frac{2I_{xy}}{I_{xx} + I_{yy}}, \quad (8)$$

and  $I_{ij}$  ( $i, j = x, y, z$ ) denotes the quadrupole moment defined by

$$I_{ij} = \int d^3x \rho x^i x^j. \quad (9)$$

Here,  $x^i = (x, y, z)$ . Simulations are performed using a 3D numerical hydrodynamic implementation in Newtonian gravity (Shibata et al. 1997) (see also Shibata 2000 for results of various test simulations with the identical hydrodynamic numerical scheme but in general relativity). We adopt a fixed uniform grid with size  $141 \times 141 \times 141$  in  $x - y - z$ , which covers an equatorial radius by 50 grid points initially. We also performed test simulations with size  $71 \times 71 \times 71$  (i.e., the grid spacing becomes twice larger) for several selected cases and confirmed that the results depend weakly on the grid resolution. We assume a reflection symmetry with respect to the equatorial plane. Since several rotating stars that we picked up have a flattened configuration, we set the grid spacing of  $z$  half of that of  $x$  and  $y$ .

#### 2.2.2 Linear stability analysis

In the linear stability analysis, we employ the scheme developed by Karino et al. (2000, 2001). The Euler perturbations of the physical quantities are replaced by functions of the form  $f(r, \theta)e^{im\varphi - i\omega t}$  in the linearized hydrodynamic equations. Here  $m$  is an azimuthal mode number. As

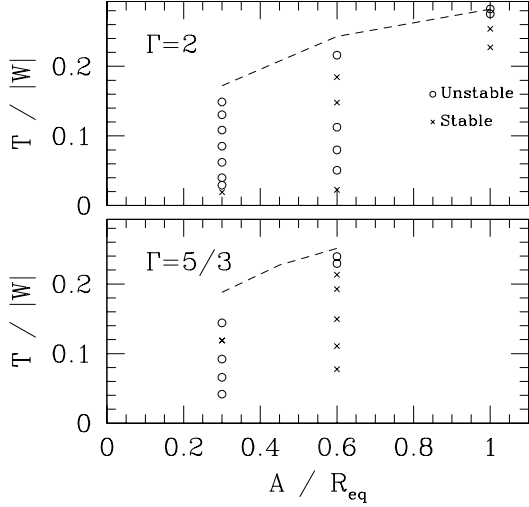


**Figure 1.** The dynamical bar-mode stability is shown in the plane of  $\beta$  and  $\hat{A}$  for the  $j$ -constant-like angular velocity profile. The circles and crosses denote that the rotating stars are unstable and stable, respectively. The dashed curves denote the boundary which distinguishes the spheroidal stars from the toroidal stars (spheroidal stars are located below the curves).

a result, the problem reduces to the eigenvalue problem for an eigenvalue  $\omega$  and the corresponding eigenfunctions of the perturbed quantities. We assume an adiabatic relation between the Euler perturbation of the pressure and that of the density. Since the fundamental mode of the  $m = 2$  or bar-type oscillations is node-less, we have checked whether the obtained eigenfunctions satisfy that condition. In this paper, we have analyzed the stability of the equilibrium configurations of  $n = 1$  polytropes for two rotation laws (1) and (2) with several values of  $\hat{A}$ .

### 3 NUMERICAL RESULTS

#### 3.1 Dynamical Bar-mode Stability

##### 3.1.1 Results by numerical simulation

The dynamical stability is studied for various combination of  $\Gamma$ ,  $\hat{A}$  and  $\beta$ , and for two angular velocity profiles in the numerical simulation. In Figures 1 and 2, we summarize the results with regard to the dynamical bar-mode stability for the  $j$ -constant-like and Kepler-like angular velocity profiles, respectively. Here, the circles (crosses) denote that the stars of a given set of  $\hat{A}$  and  $\beta$  are dynamically unstable (stable). We focus only on the spheroidal stars which are located below the dashed curves plotted in Figures 1 and 2. (If the value of  $\beta$  is larger than that on this curve for a given value of  $\hat{A}$ , the star is toroidal.)

It is found that many rotating stars of a high degree of differential rotation as  $\hat{A} = 0.1$  and  $0.3$  are dynamically unstable even for  $\beta$  of order  $0.01$ . In the case of the  $j$ -constant-like angular velocity profile, most of rotating stars with  $\beta \gtrsim 0.01$  and  $\hat{A} = 0.3$  are dynamical unstable both for  $\Gamma = 2$  and  $5/3$ . In the case of the Kepler-like angular velocity profile, the threshold of  $\hat{A}$  for onset of the instability for a given set of  $\beta$  and  $\Gamma$  appears to be slightly smaller than that

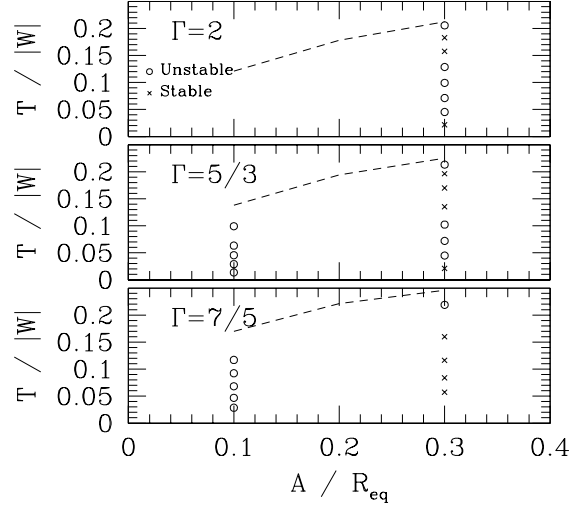


**Figure 2.** The same as Figure 1 but for the Kepler-like angular velocity profile.

in the  $j$ -constant-like case. This is because the Kepler-like angular velocity profile is not as steep as the  $j$ -constant-like one for the same value of  $\hat{A}$ . Indeed, for  $\Gamma = 2$  and  $5/3$  and for  $\hat{A} = 0.3$ , there is a wide parameter space around  $\beta \sim 0.15$  in which the stars are stable against the bar-mode deformation in the Kepler-like case. Such a wide parameter space is absent in the  $j$ -constant-like angular velocity profile for  $\hat{A} = 0.3$ . However, for  $\hat{A} = 0.1$ , the stars in a wide range of  $\beta$  are unstable even in the Kepler-like angular velocity profile. Thus, *rotating stars of a high degree of differential rotation with  $\beta$  of order  $0.01$  are dynamically unstable even in the Kepler-like angular velocity profile.*

The threshold of  $\hat{A}$  for onset of the dynamical instability for a given angular velocity profile also appears to depend on  $\Gamma$ : For a smaller value of  $\Gamma$ , the threshold of  $\hat{A}$  is smaller. For example, compare the results with  $\Gamma = 5/3$  and  $7/5$  in Fig. 2. For  $\Gamma = 5/3$ , the stars of  $\hat{A} = 0.3$  and  $0.03 \lesssim \beta \lesssim 0.1$  are unstable, but for  $\Gamma = 7/5$ , all the stars with  $\beta < 0.2$  that we studied are stable for  $\hat{A} = 0.3$ . The reason is that the rotating stars of smaller values of  $\Gamma$  have a more centrally condensed structure and as a result the effective degree of differential rotation of the central core for the stars of soft equations of state can become very high only for a sufficiently small value of  $\hat{A}$ .

The rotating stars of a high degree of differential rotation are also dynamically unstable for a high value of  $\beta$  ( $\gtrsim 0.2$ ) (see the results of  $\hat{A} = 0.6$  and  $1$  for the  $j$ -constant-like law and of  $\hat{A} = 0.3$  for the Kepler-like law). The axial ratio  $C_a$  of these stars is very small ( $C_a \lesssim 0.3$ ). In particular, for the unstable stars of the Kepler-like angular velocity profile with  $\beta \gtrsim 0.2$  and  $\hat{A} = 0.3$ ,  $C_a \sim 0.15$ . Thus, they have an almost toroidal shape. On the other hand, for the unstable stars with a small value of  $\beta$  ( $\lesssim 0.10$ ),  $C_a \gtrsim 0.5$  and, hence, the shape is not significantly toroidal.

An interesting feature is found for  $\Gamma = 2$  and  $\hat{A} = 0.6$  of the  $j$ -constant-like angular velocity profile, and for  $\Gamma = 5/3, 2$  and  $\hat{A} = 0.3$  of the Kepler-like angular velocity profile. In these cases, the stability does not change monotonically with increase of  $\beta$ : (1) stars of a sufficiently small value of

$\beta$  ( $\lesssim 0.01$ ) are stable (we have not carried out simulations for  $\beta < 0.01$ , but since the value of  $C_a$  with  $\beta \lesssim 0.01$  is larger than 0.9 (i.e., the star is almost spherical), we assume that the stars with  $\beta \lesssim 0.01$  are stable), (2) stars of  $0.01 \lesssim \beta \lesssim 0.1$  are unstable, (3) stars of  $0.1 \lesssim \beta \lesssim 0.2$  are stable again, and (4) stars of a sufficiently large value of  $\beta$  ( $\gtrsim 0.2$ ) are unstable again.

It has been widely believed that the value of  $\beta$  is a good indicator to distinguish unstable stars from stable ones. However, the examples shown here illustrate that  $\beta$  is not a good indicator for determination of the dynamical stability of rotating stars of a high degree of differential rotation.

The reason for the fact that the stability does not change monotonically with  $\beta$  is not clear. The likely reason is that the mode associated with the stability for the high value of  $\beta$  is different from that for the small value. However, this interpretation cannot be proved at present because of the following reason. The property of the unstable modes for the high value of  $\beta$  such as the perturbed density profile and the magnitude itself ( $\beta \gtrsim 0.2$ ) is essentially the same as that of the well-known bar-mode (i.e., the  $m = 2$  toroidal mode, see Chandrasekhar 1969). Hence, we identify the unstable modes of high value of  $\beta$  as the  $f$  mode. On the other hand, for the small value of  $\beta$ , the perturbed density profile is also node-less, and furthermore, the real part of the eigen frequency is approximately proportional to  $(M/R_{\text{eq}}^3)^{1/2}$  (see Figures 10 and 11). These are the properties that the  $f$  mode should have. This fact suggests that the unstable modes for the small value of  $\beta$  might be also the  $f$  mode.

We suspect that there is something different between two unstable modes of high and low values of  $\beta$ . However, to find the difference, it is necessary to precisely understand the definition of the  $f$  mode against the bar-deformation for *differentially rotating stars*. At present, it is not clear for us what properties, besides the node-less density profile and the eigen frequency of order of magnitude  $\sim (M/R_{\text{eq}}^3)^{1/2}$ , characterize the  $f$  mode. Namely, we do not know what to prove. Precisely defining the  $f$  mode for differentially rotating stars is beyond scope of this paper, and is left as a problem in future.

Before closing this section, we address the following point. As pointed out by Centrella et al. (2001), the dynamical instability for  $m = 1$  mode may set in for rotating stars of a high degree of differential rotation. In this paper, we have not found the evidence that such instability sets in. This seems to be due to the fact that we adopted only the stiff equations of state. Centrella et al. (2001) studied the instability for differentially rotating stars of a very soft equation of state with  $n = 10/3$ . In such a soft equation of state, the instability associated with the  $m = 1$  mode plays an important role. However, this is not likely the case in the stiff equations of state. Indeed, recently, Saijo et al. (2003) have pointed out that the instability of the  $m = 1$  mode sets in only for differentially rotating stars of very soft equations of state ( $n \gtrsim 2.5$ ) and of a large value of  $\beta$  ( $\gtrsim 0.15$ ).

### 3.1.2 Results by linear analysis

In Figure 3, we display the numerical results of the linear stability analysis for the same equilibrium models as shown in Figures 1 and 2 for the  $n = 1$  polytrope. These figures show that the results by the numerical simulation agree well

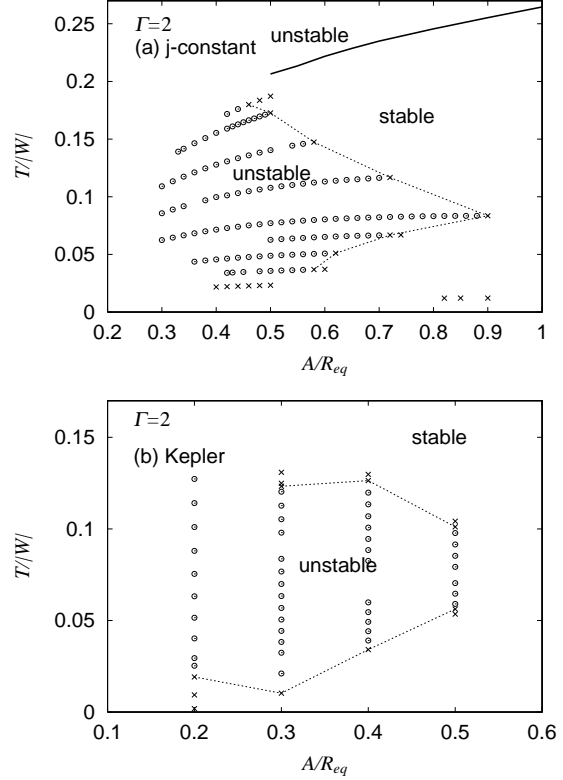


**Figure 3.** The results of the linear stability analysis are shown in the plane of  $\beta$  and  $\hat{A}$  (a) for the  $j$ -constant-like and (b) for the Kepler-like angular velocity profiles. The circles and crosses denote that the rotating stars are unstable and stable, respectively. The solid curve in the upper panel denotes the threshold of the dynamical instability against the well-known bar-mode which was calculated in Karino and Eriguchi (submitted). The dotted curves denote the approximate threshold of the stability for the small value of  $\beta$ .

with those by the linear stability analysis. This fact confirms the conclusion that rotating stars of a high degree of differential rotation are dynamically unstable even for the small value of  $\beta$  irrespective of the angular velocity profile. We note that the solid curve in the upper panel of Figure 3 denotes the threshold of the dynamical stability (i.e., above this curve the star is dynamically unstable) against the well-known bar-mode (Chandrasekhar 1969) which was calculated and reported by Karino and Eriguchi (2003).

### 3.2 Fate of unstable stars

In this section, we focus on rotating stars of the Kepler-like angular velocity profile, since the results for the  $j$ -constant-like angular velocity profile with  $\Gamma = 2$  are shown in the previous paper (Shibata et al. 2002) and, moreover, we have found that the results for  $\Gamma = 5/3$  show qualitatively identical features.

In Figures 4–7, we display time evolution of  $\eta$  as a function of  $\Omega_0 t$  for  $(\Gamma, \hat{A}) = (2, 0.3)$ ,  $(5/3, 0.3)$ ,  $(5/3, 0.1)$ , and  $(7/5, 0.1)$ . As shown here, the value of  $\eta$  does not reach the value of order 1 but saturates at order 0.1. This implies that the growth of the instability saturates at a weakly nonlin-

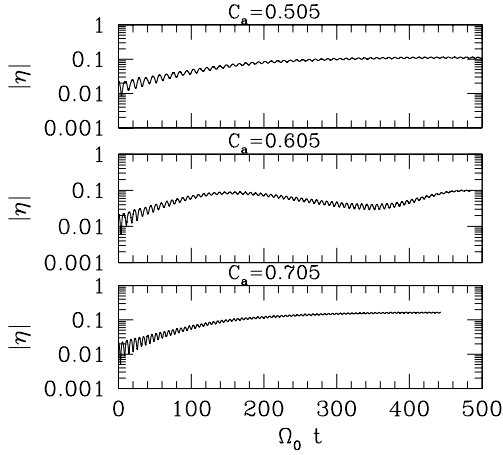


**Figure 4.** Time evolution of  $\eta$  as a function of  $\Omega_0 t$  for  $\Gamma = 2$  and  $\hat{A} = 0.3$ , and for the Kepler-like angular velocity profile.

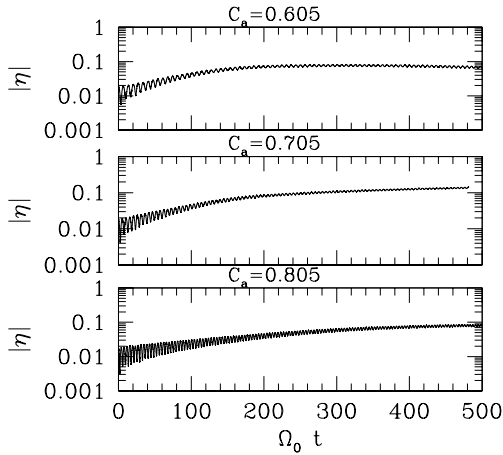


**Figure 5.** The same as Figure 4 but for  $\Gamma = 5/3$  and  $\hat{A} = 0.3$ .

ear stage. We note that for unstable stars with  $\beta \gtrsim 0.2$  and  $\hat{A} = 0.3$ , the value of  $\eta$  increases to  $\sim 1$  irrespective of  $\Gamma$ , implying that a highly deformed star is produced. There are a number of numerical works in which such a highly nonaxisymmetric structure is the outcome after onset of dynamical instability of differentially rotating stars with a high value of  $\beta$  (e.g., Williams & Tohline 1987, 1988; Houser & Centrella 1996). The outcome in the simulations for unstable stars of a high value of  $\beta$  found in the present numerical computation is qualitatively the same as that in previous papers. Thus, we do not discuss the results for such cases in the following.

After the perturbation saturates, the amplitude of  $\eta$  settles down toward a value of order 0.1. The approximate final values of  $\eta$  are

$$\eta_f \begin{cases} \sim 0.1 & \text{for } (\Gamma, \hat{A}) = (2, 0.3), \\ \lesssim 0.1 & \text{for } (\Gamma, \hat{A}) = (5/3, 0.3), \\ \sim 0.2 & \text{for } (\Gamma, \hat{A}) = (5/3, 0.1), \\ \sim 0.03 & \text{for } (\Gamma, \hat{A}) = (7/5, 0.1). \end{cases} \quad (10)$$

Comparing the results of  $(\Gamma, \hat{A}) = (5/3, 0.3)$  and  $(5/3, 0.1)$  for the identical value of  $C_a$ , it is found that for the smaller value of  $\hat{A}$ ,  $\eta_f$  is larger. This implies that a stronger degree

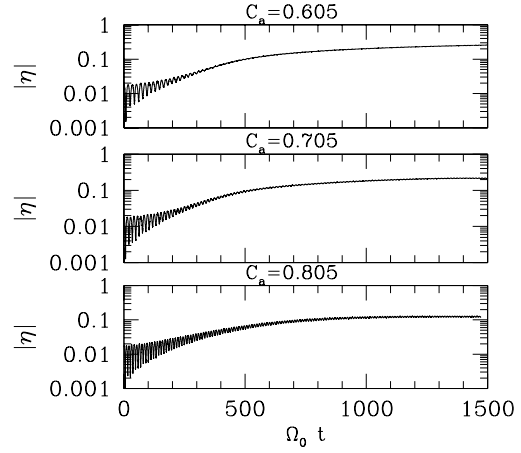


**Figure 6.** The same as Figure 4 but for  $\Gamma = 5/3$  and  $\hat{A} = 0.1$ .

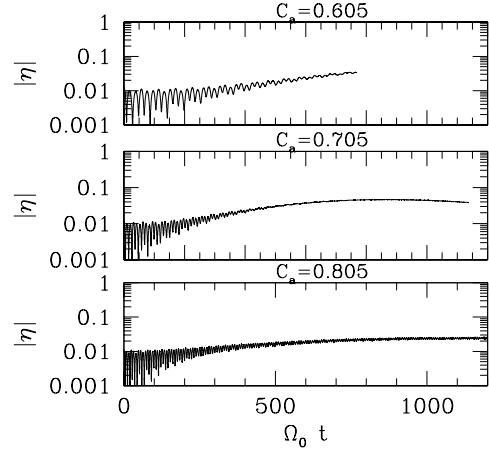


**Figure 7.** The same as Figure 4 but for  $\Gamma = 7/5$  and  $\hat{A} = 0.1$ .

of differential rotation makes the magnitude of the nonaxisymmetric deformation larger.

It is also found that for the smaller value of  $\Gamma$ , the final value of  $\eta$  is smaller. This is because the stars of smaller values of  $\Gamma$  have a more centrally-condensed structure and, hence, their effective steepness of the differential rotation is smaller for smaller value of  $\Gamma$  for a given set of  $C_a$  and  $\hat{A}$ .

In Figures 8–9, we display the snapshots of the density contour curves in the equatorial plane at selected time steps for  $(\Gamma, \hat{A}, C_a) = (2, 0.3, 0.7)$  and  $(5/3, 0.3, 0.8)$ . The value of  $\beta$  is about 0.071 and 0.045, respectively. In both cases, the nonaxisymmetric perturbation initially provided grows, changing the shape of the rotating stars to be ellipsoidal. However, the perturbation does not grow to the highly non-linear stage and, hence, neither a spiral arm nor a large bar is formed in contrast to the outcome in the simulations with a high value of  $\beta \gtrsim 0.2$ . Instead, the slightly deformed ellipsoid is the final outcome. Since the deformed ellipsoid is almost stationary,  $\eta_+$  and  $\eta_-$  oscillate quasi-periodically in the late phase of the simulations. This result is qualitatively the same as for the stars of the  $j$ -constant-like angular velocity profile (Shibata et al. 2002).

In Figures 10 and 11, we show the frequency  $f_r$  of the oscillation of the ellipsoidal star in units of  $(M/R_{\text{eq}}^3)^{1/2}$  as

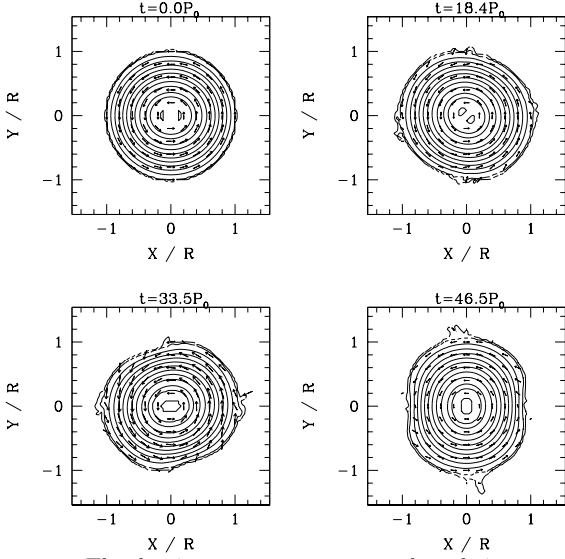


**Figure 8.** The density contour curves at selected time steps for  $\Gamma = 2$ ,  $\hat{A} = 0.3$ , and  $C_a = 0.7$  and for the Kepler-like angular velocity profile. Here,  $P_0$  is  $2\pi/\Omega_0$ . The contour curves are drawn for  $\rho/\rho_{\max} = 0.95, 0.9, 0.8, 0.7, 0.6, 0.5, 0.4, 0.3, 0.2, 0.1$  &  $0.001$ , where  $\rho_{\max}$  denotes the maximum density at each time slice. The dashed curves are plotted for  $\rho/\rho_{\max} = 0.01$  and  $0.001$ .

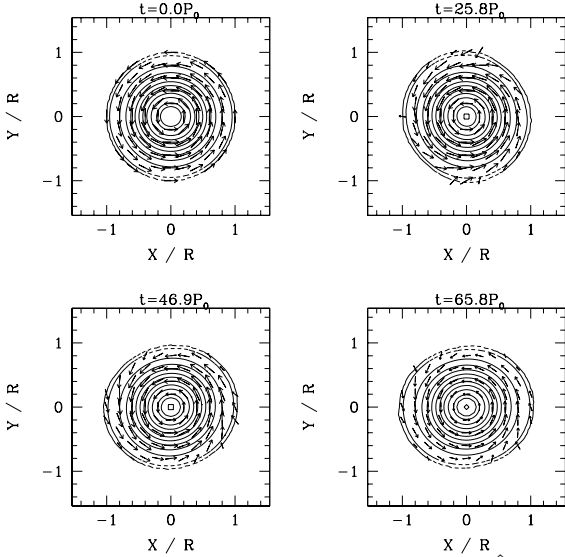


**Figure 9.** The same as Figure 8, but for  $\Gamma = 5/3$ ,  $\hat{A} = 0.3$  and  $C_a = 0.8$ .

a function of initial values of  $\beta$  for various sets of  $\Gamma$  and  $\hat{A}$ . The value of  $f_r$  is determined by the Fourier transform of  $\eta_+$  in the time domain. We note that the rotational period of the ellipsoid is  $2/f_r$ , and that the frequency of gravitational waves is  $f_r$ . It is interesting to note that for  $\Gamma = 2$  and  $5/3$ , a nondimensional quantity  $\bar{f}_r \equiv f_r(R_{\text{eq}}^3/M)^{1/2}$  is in a narrow range between 0.2 and 0.35 irrespective of  $\hat{A}$ ,  $\beta$  and angular velocity profile. For  $\Gamma = 7/5$ ,  $\bar{f}_r$  is between 0.4 and 0.55, which is larger than the values for  $\Gamma = 2$  and  $5/3$ . However, it is still in a narrow range. The fact that the value of  $\bar{f}_r$  depends weakly on  $\beta$  suggests that the excited mode may be the  $f$  mode.

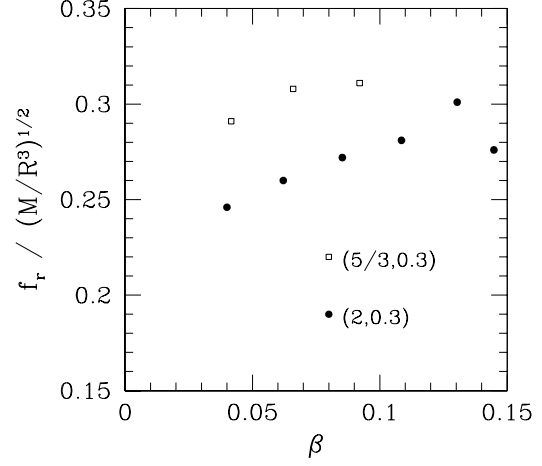


**Figure 10.**  $\bar{f}_r$  of the ellipsoids formed after onset of dynamical instability for the  $j$ -constant-like angular velocity profile. Filled circles and open squares denote the results for  $(\Gamma, \hat{A}) = (2, 0.3)$  and  $(5/3, 0.3)$ .

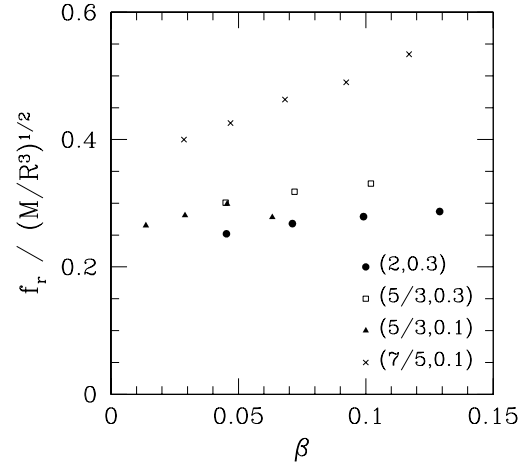


**Figure 11.** The same as Figure 10, but for the Kepler-like angular velocity profile. Filled circles, open squares, filled triangles and crosses denote the results for  $(\Gamma, \hat{A}) = (2, 0.3)$ ,  $(5/3, 0.3)$ ,  $(5/3, 0.1)$  and  $(7/5, 0.1)$ .

### 3.3 Gravitational waves

As discussed in our previous paper (Shibata et al. 2002), the dynamically unstable rotating stars, which are deformed to nonaxisymmetric ellipsoidal objects, are likely to be sources of quasi-periodic gravitational waves. In Figures 12–14, we show the gravitational waveforms of the  $+$  mode along the  $z$ -axis ( $h_+$ ) and the luminosity ( $\dot{E}$ ) as a function of time for  $(\Gamma, \hat{A}) = (2, 0.3)$ ,  $(5/3, 0.1)$  and  $(7/5, 0.1)$ . For all the models picked up here,  $C_a = 0.705$ . The value of  $\beta$  is  $\approx 0.071$ ,  $0.046$ , and  $0.047$ , respectively. We note that the waveforms for the  $\times$  mode are essentially the same as those for the  $+$  mode except for the phase difference by  $\pi/4$ . Here, we calculate gravitational waves in the quadrupole formula (Misner et al.

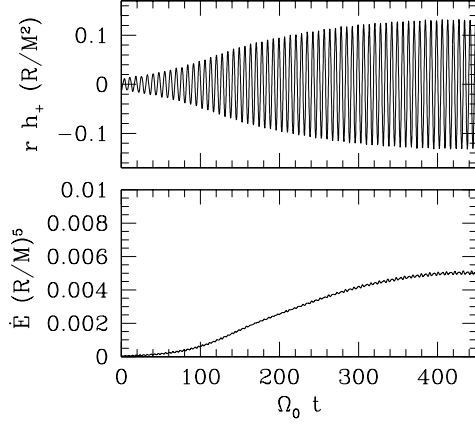


**Figure 12.** Gravitational waves for  $h_+$  in units of  $M^2/R_{\text{eq}}$  and the luminosity of gravitational waves  $\dot{E}$  in units of  $(M/R_{\text{eq}})^5$  as a function of  $\Omega_0 t$  for  $(\Gamma, \hat{A}) = (2, 0.3)$  and  $C_a = 0.705$  ( $\beta \approx 0.071$ ).

1973) and define the waveforms by

$$h_+ \equiv \frac{\ddot{I}_{xx} - \ddot{I}_{yy}}{r}, \quad h_\times \equiv \frac{2\ddot{I}_{xy}}{r}, \quad (11)$$

and the luminosity by

$$\dot{E} \equiv \frac{1}{5} \sum_{i,j} \mathcal{I}_{ij}^{(3)} \mathcal{I}_{ij}^{(3)}, \quad (12)$$

where

$$\mathcal{I}_{ij} = I_{ij} - \frac{\delta_{ij}}{3} \sum_k I_{kk},$$

$$\ddot{I}_{ij} = \frac{d^2 I_{ij}}{dt^2}, \quad \mathcal{I}_{ij}^{(3)} = \frac{d^3 \mathcal{I}_{ij}}{dt^3}, \quad (13)$$

and  $r$  is the distance from a source to a detector.  $h_+$  and  $h_\times$  are the waveforms observed along the  $z$  axis.

In the early phase before the growth of the nonaxisymmetric perturbation saturates, the amplitude of gravitational waves increases gradually together with the magnitude of  $\eta$ . Then, the growth of the amplitude saturates and subsequently, quasi-periodic gravitational waves are emitted for a much longer time than the rotational period. The amplitude of quasi-periodic gravitational waves depends on  $\Gamma$  and  $\hat{A}$ , as in the case of the saturated value of  $\eta$ . For a given set of  $\hat{A}$  and  $C_a$  (or  $\beta$ ), it is smaller for smaller values of  $\Gamma$ . This is because the star with smaller values of  $\Gamma$  is more centrally condensed and, hence, the magnitudes of the quadrupole moments are smaller for the identical mass and radius.

We found that for the parameters we studied ( $\beta \lesssim 0.1$ ,  $\hat{A} \leq 0.6$  and angular velocity profiles (1) and (2)), the typical values of the amplitude and luminosity of gravitational waves for  $\Gamma = 2$  are  $rh_{+, \times} \sim 0.1\text{--}0.2(M^2/R_{\text{eq}})$  and  $\dot{E} \sim 0.005\text{--}0.01(M/R_{\text{eq}})^5$ . For  $\Gamma = 5/3$ , the magnitudes of them are only slightly smaller than those for  $\Gamma = 2$ . However, for  $\Gamma = 7/5$ , they are smaller by a factor of several as  $rh_{+, \times} \sim 0.05(M^2/R_{\text{eq}})$  and  $\dot{E} \sim 0.001(M/R_{\text{eq}})^5$ .

Using the results shown in Figures 12–14, we can estimate the expected effective amplitude of gravitational waves from the nonaxisymmetric outcomes formed after the dynamical instability saturates. Here, we pay particular at-

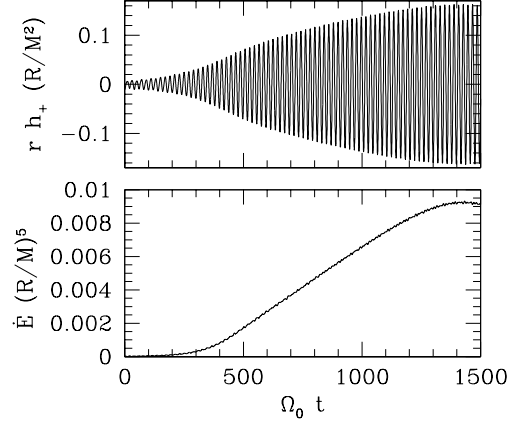


**Figure 13.** The same as Figure 12, but for  $(\Gamma, \hat{A}) = (5/3, 0.1)$  and  $C_a = 0.705$  ( $\beta \approx 0.046$ ).

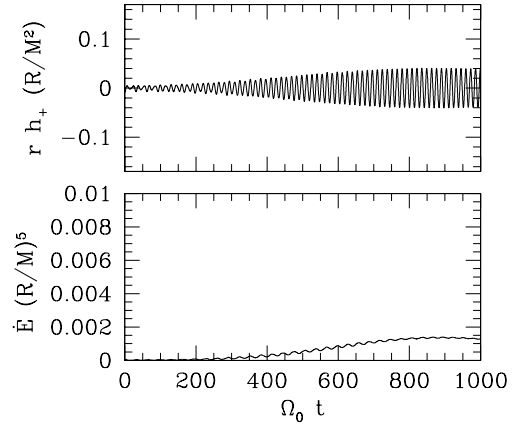


**Figure 14.** The same as Figure 12, but for  $(\Gamma, \hat{A}) = (7/5, 0.1)$  and  $C_a = 0.705$  ( $\beta \approx 0.047$ ).

tention to proto-neutron stars which are likely formed soon after the supernovae of mass  $\sim 1.4M_\odot$  and radius several 10 km. For the luminosity  $\dot{E} = 0.001\epsilon(M/R_{\text{eq}})^5$  where  $\epsilon$  is a parameter of magnitude 1–10, the emission timescale of gravitational waves can be estimated as

$$\begin{aligned} \tau \sim \frac{T}{\dot{E}} &= 100\alpha_0\epsilon^{-1} \left(\frac{\beta}{0.1}\right) \left(\frac{R_{\text{eq}}}{M}\right)^4 M \\ &= 6.1 \text{ sec } \alpha_0\epsilon^{-1} \left(\frac{\beta}{0.1}\right) \left(\frac{R_{\text{eq}}}{30 \text{ km}}\right)^4 \left(\frac{M}{1.4M_\odot}\right)^{-3} \end{aligned} \quad (14)$$

where we set  $T = \alpha_0\beta M^2/R_{\text{eq}}$ , and  $\alpha_0$  is a constant which depends on the value of  $\Gamma$  but very weakly on  $\hat{A}$ ; for  $\beta \lesssim 0.1$ ,  $\alpha_0 \sim 0.8, 0.9$ , and  $1.2$  for  $\Gamma = 2, 5/3$ , and  $7/5$ , respectively, within  $\sim 10\%$  error.

The characteristic frequency of gravitational waves is denoted as

$$f = f_r \approx 790 \text{ Hz} \left(\frac{\bar{f}_r}{0.3}\right) \left(\frac{R_{\text{eq}}}{30 \text{ km}}\right)^{-3/2} \left(\frac{M}{1.4M_\odot}\right)^{1/2}. \quad (15)$$

Assuming that the nonaxisymmetric perturbation would not be dissipated by viscosities or magnetic fields on the emis-

sion timescale of gravitational waves (e.g., Baumgarte et al. 2000), the accumulated cycles of gravitational wave-train  $N$  are estimated as

$$N \equiv f\tau = 4.8 \times 10^3 \alpha_0 \left(\frac{\epsilon}{5}\right)^{-1} \left(\frac{\bar{f}_r}{0.3}\right) \times \left(\frac{\beta}{0.1}\right) \left(\frac{R_{\text{eq}}}{30 \text{ km}}\right)^{5/2} \left(\frac{M}{1.4M_\odot}\right)^{-5/2}. \quad (16)$$

The effective amplitude of gravitational waves is defined by  $h_{\text{eff}} \equiv N^{1/2}h$  where  $h$  denotes the characteristic amplitude of periodic gravitational waves. Using this relation, we find

$$h_{\text{eff}} \approx 3.2 \times 10^{-22} \alpha_0^{1/2} \left(\frac{\bar{h}}{0.1}\right) \left(\frac{\epsilon}{5}\right)^{-1/2} \left(\frac{\beta}{0.1}\right)^{1/2} \left(\frac{\bar{f}_r}{0.3}\right)^{1/2} \times \left(\frac{R_{\text{eq}}}{30 \text{ km}}\right)^{1/4} \left(\frac{M}{1.4M_\odot}\right)^{3/4} \left(\frac{100 \text{ Mpc}}{r}\right) \quad (17)$$

(Thorne 1987; Lai & Shapiro 1995; Liu & Lindblom 2001; Liu 2002) where  $\bar{h} \equiv hrR_{\text{eq}}/M^2$ . Since  $\bar{f}_r$ ,  $\bar{h}$ ,  $\epsilon$  and  $\beta$  depend on the values of  $\Gamma$ ,  $\hat{A}$ , and  $C_a$ ,  $h_{\text{eff}}$  can vary by a factor of  $\sim 3$ . However, for all the rotating stars that we studied in this paper,  $h_{\text{eff}}$  is always larger than  $10^{-22}$  at a distance  $r \sim 100$  Mpc with  $R_{\text{eq}} \sim 30$  km and  $M \sim 1.4M_\odot$ . Furthermore, the frequency of gravitational waves is about 1 kHz for  $R_{\text{eq}} \sim 30$  km and  $M \approx 1.4M_\odot$ . Thus, gravitational waves from proto-neutron stars of a high degree of differential rotation, of mass  $\sim 1.4M_\odot$ , and of radius  $\gtrsim 30$  km at a distance of  $\sim 100$  Mpc are likely to be sources for laser interferometric detectors such as LIGO (Thorne 1995), if the other dissipation processes are negligible.

#### 4 SUMMARY AND DISCUSSION

We have studied the dynamical bar-mode instability of differentially rotating stars of polytropic equations of state. We chose three polytropic indices and two angular velocity profiles in this study. We found that rotating stars of a high degree of differential rotation are dynamically unstable against the nonaxisymmetric bar-mode deformation even with  $\beta \ll 0.27$ , irrespective of the polytropic indices and angular velocity profile. The criterion of the value of  $\beta$  for onset of the instability depends on the rotational profile and the equations of state, but the dependence is very weak if the degree of differential rotation is high enough as  $\hat{A} \sim 0.1$ .

We estimated the effective amplitude of gravitational waves from nonaxisymmetric objects formed after onset of the dynamical instability. For typical proto-neutron stars of mass  $\sim 1.4M_\odot$  and radius several 10 km, the effective amplitude of gravitational waves at a distance of  $\sim 100$  Mpc is larger than  $10^{-22}$ , and the frequency  $\sim 1$  kHz. Therefore, the gravitational waves can be sources for laser interferometric detectors such as advanced LIGO (e.g., Thorne 1995).

As we mentioned above, this conclusion is drawn under the assumption that dissipation of nonaxisymmetric perturbations by viscosity and magnetic fields is negligible. The dissipation timescale due to molecular viscosities and magnetic braking is likely to be longer than 10 sec (e.g., Baumgarte et al. 2000). Thus, these effects can be safely neglected. However, turbulent magnetic viscosity (Balbus & Hawley

1998) may be relevant for redistribution of the angular momentum profile. This implies that a differentially rotating star might be enforced to a rigidly rotating state on a dynamical timescale and, hence, the nonaxisymmetric structure might disappear. Many theoretical works have clarified that the magnetic viscous effect can redistribute the angular momentum distribution of accretion disks around central objects on a dynamical timescale (Balbus & Hawley 1998). However, to our knowledge, there is no work on the magnetic field effect to self-gravitating rotating stars. The magnetic field would redistribute the angular momentum of the differentially rotating stars on a dynamical timescale, but it is not clear if it is strong enough to enforce the rotating stars to an axisymmetric state in a dynamical timescale. To clarify this problem, it is necessary to carry out MHD simulations for rotating stars. Such work should be done in the future.

#### ACKNOWLEDGMENTS

We thank L. Lindblom and I. Hachisu for discussion and comments. Numerical simulations were performed on FACOM VPP5000 in the data processing center of National Astronomical Observatory of Japan. This work was in part supported by a Japanese Monbu-Kagaku-Sho Grant (Nos. 12640255, 13740143 and 14047207). SK is supported by JSPS Research Fellowship for Young Scientists.

#### REFERENCES

- Andalib, S. W., Tohline, J. E., Christodoulou, D. M. 1997, ApJS, 108, 471
- Baumgarte, T. W., Shapiro, S. L., Shibata, M., 2000, ApJL, 528, L29
- Balbus, S. A., Hawley, J. F., 1998, Rev. Mod. Phys., 70, 1
- Centrella, J. M., New, K. C. B., Lowe, L., Brown, J. D., 2001, ApJL, 550, 193
- Chandrasekhar, S., 1969, Ellipsoidal Figures of Equilibrium, Yale University Press, New Haven.
- Goodman, J., Narayan, R. 1988, MNRAS, 231, 97
- Houser, J. L., Centrella, J. M., 1996, Phys. Rev. D., 54, 7278
- Karino, S., Eriguchi, Y., submitted to ApJ.
- Karino, S., Yoshida, S'i., Yoshida, S'j., Eriguchi, Y., 2000, Phys. Rev. D., 62, 084012
- Karino, S., Yoshida, S'i., Eriguchi, Y., 2001, Phys. Rev. D., 64, 024003
- Lai, D., Shapiro, S. L., 1995, ApJ, 442, 259
- Liu, Y. T., Lindblom, L., 2001, MNRAS, 342, 1063
- Liu, Y. T., 2002, Phys. Rev. D., 65, 124003
- Misner, C. W., Thorne, K. S., Wheeler, J. A., 1973, Gravitation, W. H. Freeman and Company, New York
- Papaloizou, J.C.B., Pringle, J.E. 1984, MNRAS, 208, 721
- Saijo, M., Baumgarte, T. W., Shapiro, S. L., astro-ph/0302436
- Shibata, M., Oohara, K., Nakamura, T., 1997, Prog. Theor. Phys., 98, 1081
- Shibata, M., 2000, Phys. Rev. D., 60, 104052
- Shibata, M., Karino, S., Eriguchi, Y., MNRAS, 334, L27
- Thorne, K. S., 1987, 300 Years of Gravitation, eds. Hawking, S., Israel, W., Cambridge University Press, Cambridge, 330
- Thorne, K. S., 1995, Proceeding of Snowmass 95 Summer Study on Particle and Nuclear Astrophysics and Cosmology, eds. Kolb, E. W., Peccei, R., World Scientific, Singapore, 398
- Tohline, J. E., Hachisu, I., 1990, ApJ. 361, 394
- Williams, H. A., Tohline, J. E., 1987, ApJ. 315, 594



Williams, H. A., Tohline, J. E., 1988, ApJ. 334, 449